

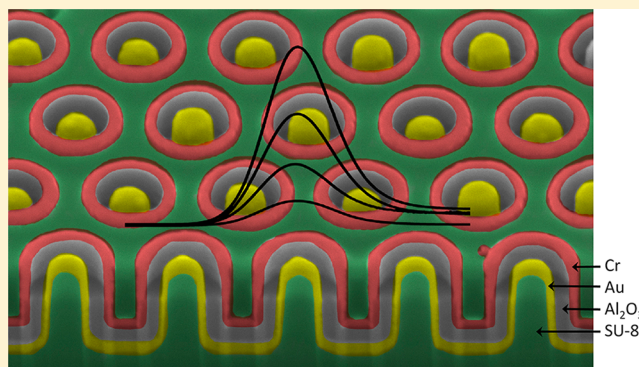
Nanocoax-Based Electrochemical Sensor

Binod Rizal,[†] Michelle M. Archibald,[‡] Timothy Connolly,[‡] Stephen Shepard,[§] Michael J. Burns,[†] Thomas C. Chiles,[‡] and Michael J. Naughton^{*†}

[†]Department of Physics, [‡]Department of Biology, [§]Integrated Sciences Cleanroom Facility, Boston College, Chestnut Hill, Massachusetts 02467, United States

S Supporting Information

ABSTRACT: We have used a facile polymer imprint process to fabricate a three-dimensional electrochemical nanosensor, the sensitivity of which is two decades higher than that of planar controls. The device is composed of an array of vertically oriented nanoscale coaxial electrodes, with the coax cores and shields serving as integrated working and counter electrodes, respectively, each with a nanoscale separation gap (coax annulus width). Arrays of $\sim 10^6$ devices per square millimeter were prepared with different gaps, with smaller gaps yielding higher sensitivity. A coax-based sensor with a 100 nm gap was found to have sensitivity 90 times greater than that of a planar sensor control, which had conventional millimeter-scale electrode gap spacing. We suggest that this enhancement is due to the combination of rapid diffusion of molecules between the closely spaced electrodes and the large number of nanoscale electrochemical cells operating in parallel, both of which enhance current per unit surface area compared to planar or other nanostructured devices.



Considerable effort has been directed toward increasing target sensitivity in electrochemical sensors (ES) by developing “nanogap” electrodes that can provide real-time ultrasensitive detection of chemical and biological agents. Reduction of the distance between the electrodes has received considerable attention as this is thought to improve mass transport and Faradic-to-capacitive signal ratio, as well as decrease the response time and the effect of the solution resistance.^{1–6} Lithographic techniques such as electron-beam,^{7–9} dip-pen,¹⁰ transmission electron beam ablation,¹¹ and focused ion beam (FIB) milling^{12,13} can be used to make nanoscale gap electrodes. However, these methods are commonly used for planar, two-dimensional structures and are inevitably serial, costly, and time-consuming processes. Other techniques such as electromigration,^{14,15} electrochemical deposition,^{16,17} and electro-breakdown¹⁸ are simpler and faster than the aforementioned techniques for planar nanogap electrode fabrication, but have limited flexibility in controlling the size and shape of the gap between the electrodes. Although different methods have been developed, it remains a challenge to fabricate highly ordered arrays of nanogap electrodes with confined geometries over a large area and to do so in a reproducible and cost-effective manner. We have developed a simple and reliable method for fabricating highly ordered arrays of electrodes with well-defined nanogaps over a large area for use in ES devices, maintaining the advantage of nanogap sensing while overcoming previous limitations. No formal lithographies (photo- or electron beam) are employed in the fabrication.

Our design for a simple, miniaturized ES consists of arrays of vertically oriented coaxial electrodes, termed “nanocoaxes”. Variants of this structure have previously been employed in nanophotonic,^{19,20} photovoltaic,^{21,22} and capacitance-based chemical sensing²³ applications. It consists of two concentric electrodes separated by a dielectric layer or air gap. We fabricated ESs using these two electrodes as the working electrode (WE) and counter electrode (CE). ES arrays with different electrode gaps were prepared by changing the thickness of the dielectric layer and then removing it, with the resulting effect on the Faradic current examined via differential pulse voltammetry (DPV).

EXPERIMENTAL SECTION

Chemicals. 1H,1H,2H,2H-Perfluorodecyltrichlorosilane (96%) and *n*-heptane (99%) were purchased from Alfa Aesar. Acetone (99.5%), sulfuric acid (96%), and hydrogen peroxide (30%) were purchased from J.T. Baker. Polydimethylsiloxane (Sylgard 184 silicone elastomer kit) was purchased from Dow Corning. SU-8 2002 was purchased from MicroChem Corp. Transetch-N was purchased from Transene Co. Ferrocene carboxylic acid was purchased from Sigma-Aldrich. Phosphate buffered saline was purchased from Fisher Scientific.

Received: August 2, 2013

Accepted: October 3, 2013

Published: October 3, 2013

Preparation of Silicon Nanopillar Arrays. Silicon nanopillar (SiNP) arrays were prepared by a combination of thermal oxidation and reactive ion etching of [100] silicon substrates that were photolithographically patterned. Typical SiNP dimensions were 2 μm height and 200 nm diameter, with hexagonal close-packed arrays of 1.3 μm periodicity/pitch, on substrates containing $10 \times 20 \text{ mm}^2$ areas of pillars. This results in a pillar density of approximately $10^6/\text{mm}^2$.

Application of Release Coating. A release coating was applied to the SiNP arrays, which were used as imprint masters. The master array was immersed in a solution containing 1*H*,1*H*,2*H*,2*H*-perfluorodecyltrichlorosilane (FDTs) and *n*-heptane in the ratio of 1:1000 (v/v), followed by immediate transfer of the master to acetone for another 5 min, and then baked for 5 min at 110 $^\circ\text{C}$ on a hot plate. The measured thickness of the FDTs using ellipsometry (J.A. Woollam VASE) was $1.76 \text{ nm} \pm 0.12 \text{ nm}$, which is comparable to the previously reported value for a single layer of FDTs.²⁴

Fabrication of Molds. Polydimethylsiloxane (PDMS) was mixed in the ratio of 10:1 (w/w) with its curing agent and degassed in a bell-jar desiccator connected to a vacuum pump for 30 min. It was then poured onto the Si master, cured at room temperature for 12 h, and baked for 1 h on a hot plate at 90 $^\circ\text{C}$. The PDMS mold was then peeled off and treated with release coating and used for imprinting in subsequent steps. Typical thickness of the PDMS mold was $\sim 2 \text{ mm}$.

Imprinting of SU-8 Pillar Arrays. A thin film of SU-8 2002 was spin-coated on a piranha-cleaned Si wafer at 500 rpm with acceleration of 110 rpm/s for 6 s and then at 3000 at 550 rpm/s for 36 s, followed by soft baking at 65 $^\circ\text{C}$ for 1 min and at 95 $^\circ\text{C}$ for at least 2 min to remove any residual solvent. The film was cooled to room temperature, and the mold was placed on top of it. To ensure conformal contact between the mold and the film, an overpressure of $\sim 10^5 \text{ Pa}$ was applied between them using a homemade apparatus. The PDMS mold and SU-8 were then held at 95 $^\circ\text{C}$ on a hot plate for 5 min and exposed to UV light in a mask aligner (MA6, Karl Suss) at $12 \text{ mW}/\text{cm}^2$ for 90 s. A postexpose bake was then done for 5 min, and the sample was allowed to cool to room temperature before peeling off the PDMS elastomer mold to release the now-formed SU-8 nanopillar array.

Fabrication of Hollow Nanocoax Arrays. A thin film ($\sim 125 \text{ nm}$) of Au was deposited as the SU-8 pillar array (to later serve as the coax inner conductors) using sputter deposition (AJA International) with 250 W dc power and 0.75 nm/s deposition rate. Atomic layer deposition (ALD) (Savannah S100, Cambridge Nanotech) was then used to deposit Al_2O_3 at 200 $^\circ\text{C}$ (to serve as coax annulus), followed by a second sputter deposition of $\sim 150 \text{ nm}$ of Cr (for the outer coax conductor) with 200 W dc power and 0.1 nm/s deposition rate. A second layer of SU-8 was then spin-coated onto this newly formed coax array, followed by UV exposure at $12 \text{ mW}/\text{cm}^2$ for 90 s and a hard bake at 200 $^\circ\text{C}$ for 1 h. This is to provide mechanical support for the nanocoaxes. A mechanical polisher (Vibromet 2, Buehler) with a suspension of 50 nm diameter alumina nanoparticles was used for 2.5 h to remove the top part of the outer metal of the coax. After this decapitation, the Al_2O_3 in the annuli of the coaxes was etched to a time-controlled depth at room temperature at a rate of $\sim 20 \text{ nm}/\text{h}$ by immersion in Transetch-N.

Characterization. Scanning electron microscope (SEM) images of the pillar and coax arrays were taken using a JEOL JSM-7001F SEM. FIB milling was done on a JEOL JIB-4500

FIB. The thicknesses of the thin films were measured by a profilometer (Dektak 150, Veeco). Electrochemical characterization was performed using a potentiostat (Reference 600, Gamry Instruments).

RESULTS AND DISCUSSION

We employed the above stamp imprint method in the fabrication of our nanocoax array electrochemical cells. Imprinting (also referred to as soft lithography or nanoimprint lithography²⁵) is a useful technique for rapid and cost-effective replication of micro- and nanostructures, including those with 3D features such as the vertical nanopillar arrays of interest here. Aside from its nanoscale capability, perhaps the greatest advantage of the imprinting technique is its ability to produce a large number of large area replicas with high fidelity from a single master. We thus used imprint-prepared nanopillar arrays as the basis for the fabrication of vertically oriented nanocoax arrays.¹⁹ For the imprint masters, we used SiNP arrays prepared as above. We used SU-8 photoresist for the nanopillar replicas for its relatively low glass transition temperature and volume shrinkage coefficient and its wide range of operating temperatures. After fabricating nanocoax arrays as ESs, we used them to explore the effect of the working-counter electrode gap on the Faradic current of the device.

Figure 1 depicts SEM images of a representative SiNP master and SU-8 replica. To form arrays of nanocoaxes, the first step is

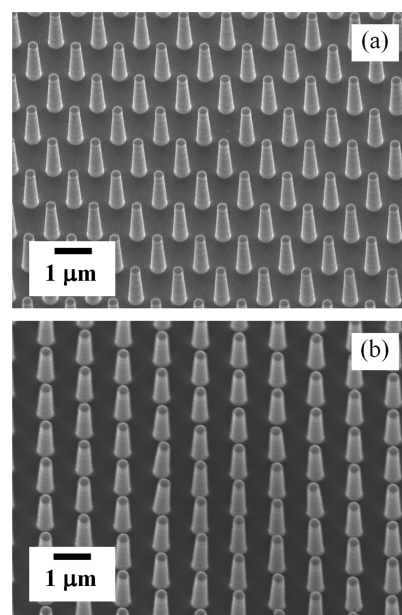


Figure 1. SEM images of arrays of (a) 2 μm tall Si nanopillars of period 1.3 μm prepared via lithographic techniques followed by chemical etching for use as a master for imprinting and (b) SU-8 replica of the master made using a PDMS mold.

metallization of the SU-8 NPs, to serve as the coax cores. After this initial metallization, we deposited a dielectric layer to function as the coax annulus, followed by a second metal deposition to act as the coax shield. To use the coax structure as an ES, the top part of the outer metal was removed by polishing, exposing the dielectric core. These arrays were further processed by partially wet etching the annuli of the coaxes to open a cavity between the coax inner and outer electrodes, into which an analyte solution can ultimately fill and

be detected, as depicted in Figure 2. Further fabrication details can be found in the Supporting Information.

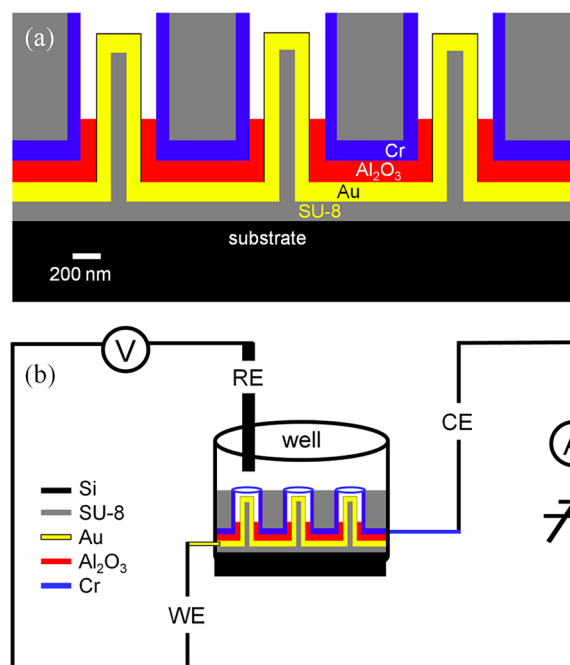


Figure 2. Schematic representations of (a) a partially hollowed nanocoax array and (b) a coax-based ES made using inner and outer electrodes of the coax array as WE and CE, respectively, of an ES.

We sputter-deposited 120 nm of Au for the metallization of the SU-8 nanopillars. To improve conformality of the coating, we used conical rather than strictly vertical nanopillars, as shown in Figure 1. For the dielectric layer, we deposited aluminum oxide (Al_2O_3) of defined thickness, typically 100 to 400 nm, by ALD. In ALD, trimethylaluminum is used as the organometallic precursor with a 200 °C deposition temperature. Next, a Cr film of ~ 150 nm thickness was sputtered as an outer metal to form the nanocoaxial structure. Depending on pillar height, the horizontal thickness of the metal on the walls of the conical pillars typically ranged from 1/3 to 1/2 that of the vertical thickness of the metal at the base between pillars.

Before polishing, an important consideration is structural support for the nanocoaxes in the arrays. This was provided by coating the array with a second SU-8 stabilizing layer, filling the space between coaxes to a thickness comparable to or greater than the height of the array. Mechanical polishing was then performed using suspensions of Al_2O_3 nanoparticles on a vibratory polisher. Polishing/SEM inspection cycles continued until the outer metal on the top of coaxes was fully removed, thus exposing the Al_2O_3 annuli. The dielectric in the annulus was removed by wet etching with Transetch-N solution at room temperature, yielding a cavity of ~ 500 nm vertical depth into the annulus. Figure 3 shows SEM images of nanocoax arrays of $1.3 \mu\text{m}$ pitch, 200 nm annulus thickness, and ~ 500 nm annulus depth, as well as a cross-sectional view of a portion of an array obtained by FIB milling. We have fabricated similar arrays with annulus thickness ranging from 100 to 400 nm to investigate the effect of electrode separation on subsequent ES performance.

After fabrication, arrays of coaxes were isolated using a custom-made polypropylene gasket to create a reservoir for

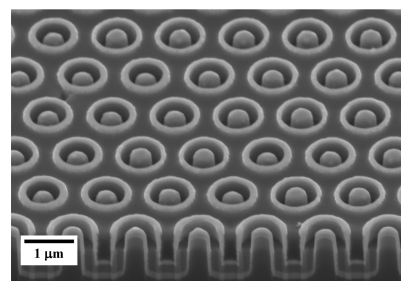


Figure 3. SEM image of an array of partially hollow nanocoaxes of $1.3 \mu\text{m}$ pitch, 200 nm annulus thickness, and 500 nm annulus depth with Au inner and Cr outer electrodes. Bottom portion shows a cross-section of one row of the array prepared by FIB milling.

liquid on top of the arrays. The reservoir (or well) was filled with a redox reagent, 1 mM ferrocene carboxylic acid (FCA) in phosphate buffered saline (PBS). A three-electrode ES was then configured by using the inner and outer coax electrodes as the WE and CE, respectively, and a Ag/AgCl electrode immersed in the reservoir as a reference electrode (RE), as shown in Figure 2. For comparative study, we also constructed an ES with a planar Au WE, Pt CE, and Ag/AgCl RE (not shown), which had the same projected WE area as the coax arrays (1.8 mm^2).

For analytical purposes, DPV was employed as the electrochemical measurement technique. A factor which plays an important role in reducing the background charging current in pulse techniques, especially at higher measuring speeds, is the RC-time constant of an electrochemical cell. This is defined by the factor $R_u C_d$, where R_u is the uncompensated resistance, and C_d is the double layer capacitance. The maximum value of uncompensated resistance of an electrolyte solution of conductivity σ , confined between two electrodes separated by a distance d , is $R_u = d/\sigma A$, where A is the area of the inner electrode. There is an electric double layer capacitance density C_d due to the charged species and oriented dipoles at the metal–solution interface, whose typical value is in the range of $10\text{--}40 \mu\text{F}/\text{cm}^2$.⁵ For a physiological solution such as PBS of bulk conductivity $0.14\text{--}0.18 \text{ S/m}$,²⁶ the value of uncompensated resistance R_{ui} for a nanocoax with 250 nm diameter inner electrode, 200 nm annulus width, and 500 nm diameter is $R_{ui} \sim 3 \text{ M}\Omega$. The number of coaxes within a 1.5 mm diameter array area is $n \sim 1.2 \times 10^6$. For resistive analysis, coax arrays can be treated as a parallel combination of n resistors, with an equivalent resistance $R_u = R_{ui}/n \sim 1 \Omega$. For such arrays, we calculate the value of the double layer capacitance to be $C_d \sim 0.1 \mu\text{F}$. With these values, the cell RC-time constant of a nanocoax ES within the 1.5 mm diameter area employed is $\sim 10^{-7} \text{ s}$. For comparison, the RC-time constant of a planar cell with the WE and CE separated by mm-scale distance is $\sim 10^{-3} \text{ s}$.

Following the standard practice of using a DPV pulse time ~ 10 times greater than the RC-time constant, the coax-based ES reduces the limit of the experimental time scale to 10^{-6} s ($1 \mu\text{s}$) for the commonly used biological medium PBS. Such a rapid time scale could only be achieved for other microstructures by using a medium with high electrical conductivity.²⁷ Thus, the low value of the time constant of the coax-based ES provides the unique ability to study voltammetric signals in media with low conductivity. In principle, an ES with a time of $\sim 1 \mu\text{s}$ can also be used to measure the redox potentials of highly reactive intermediates and the rate constant of rapid

heterogeneous charge transfer, as well as to analyze complex mechanisms including chemical steps.^{28–32}

To observe the effect of electrode (WE–CE) separation on Faradic current, DPV measurements were carried out using initial and final potentials of 0.0 and 0.5 V, respectively, pulse size of 50 mV, pulse time of 0.05 s, step size of 2 mV, and sample period of 0.1 s, for the redox chemical 1 mM FCA in PBS. Measured values of coax-based ESs with different electrode gaps (coax annulus widths) are shown in Figure 4,

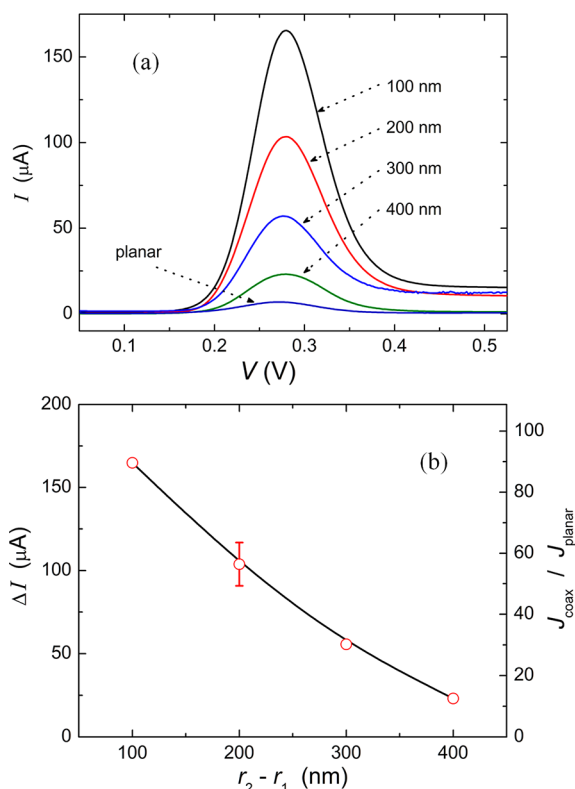


Figure 4. DPV signal from different annulus thickness, coax-based electrochemical sensors. (a) Current in nanocoax-based ES with 100 to 400 nm gaps between WE and CE, plotted vs. WE potential. Data for a planar ES control having millimeter-scale WE–CE gap is also shown. (b) Left axis: Difference between peak current and current at 0.1 V WE potential vs. gap ($r_2 - r_1$) between WE and CE for nanocoax-based ES. Right axis: Ratio of current density in coax-based ES cell to that in planar ES vs. gap between WE and CE of nanocoax-based ES.

as well as results for the planar WE cell. Figure 4a shows that all coax and planar ESs had a well-defined peak at 280 mV vs. (Ag/AgCl), which corresponds to the redox reaction of FCA. The width of the peak at half height for all curves is $\delta I_{1/2} \sim 92$ mV, close to a previously reported value of 90.4 mV^{33,34} for a one electron process at 25 °C. However, in all cases, the coax-based devices displayed higher current than the planar control. In Figure 4b, we show the dependence of the peak value of the current on the coax-based WE–CE separation $d = r_2 - r_1$, where r_1 is the outer radius of the inner coax conductor and r_2 is the inner radius of the outer coax conductor. For consistency of measurement for all values of electrode separation, we subtracted the background current at 0.1 V from the peak current value, indicated as ΔI in Figure 4b. This is less than a 1% effect on the overall result. The current at $d = 200$ nm is the average of three identically prepared ES arrays, with the error bar indicating the standard deviation. As anticipated, the value

of the peak current increases inversely with decreasing distance between electrodes. This can be explained by assuming a linearly varying concentration gradient of the redox molecules within the diffusion layer between the two electrodes. Under this condition, current can be expressed⁵ as $I \sim (r_2 - r_1)^{-1}$. The ratio of current density for the coax-based ES to that for the planar device is also shown in Figure 4b. The coax-based ES with 100 nm electrode gap is seen to have a signal nearly 2 orders of magnitude greater than that of the conventional, planar ES (i.e., $J_{\text{coax}}/J_{\text{planar}} = 90$), while the noise level in each ES is approximately the same.

We suggest that the observed improvement in signal-to-noise ratio in the coax-based ES compared to the planar ES, and with decreasing electrode gap in the coax-based ES, is due to two effects: rapid diffusion of redox species between the closely spaced electrode surfaces and the large number of nanocoaxes in our device. The small gap between the WE and CE facilitates efficient diffusion of redox molecules between electrodes, with the result that species reduced at the counter electrode rapidly return back to the working electrode and vice versa, providing positive feedback to the signal.^{35–37} This process presents a large flux of redox species between electrodes, which yields a higher value of current compared to a sensor with a large electrode gap. The small dimensions of each nanocoax and their close spacing is such that each 1.5 mm diameter ES device contains more than 10^6 nanocoax ESs operating in parallel (whose signals are thus additive). Also, in this coaxial structure, the inner electrode is circumferentially surrounded by the outer electrode, such that molecules always diffuse radially (i.e., horizontally) between the electrodes. In combination, this means that we are within the linear diffusion regime such that the electrochemical processes are not mass diffusion limited, a problem found in other nanogaps ES devices.⁸ This is evidenced by a conventionally shaped cyclic voltammogram (not shown), in contrast to peak-shaped curves in the planar-diffusion dominated nanodevices.⁸

While our devices are in array form, one can employ smaller subarrays or even individual coaxes as a micro- or nanoscale ES, after electrically addressing each coax or subarray. Such a device could then be employed, for example, to map variations in local concentration of the brain-signaling molecules in vitro/silico/vivo, which could be more facile and sensitive than the traditional manner of monitoring the concentration of the molecules using ultramicroelectrodes.³⁸ In addition, with further development to incorporate microfluidics for liquid exchange, the coax device could be developed into a cost-effective, portable device for rapid molecular analysis in broader applications such as environmental monitoring of chemicals and toxins, pathogen detection, and biomarker detection for the diagnosis of human disease, such as early stage cancer. As the open volume (in the hollow annulus) of each nanocoax is ~ 50 aL, very small analyte volumes could be employed (e.g., 1 fL for a 5×5 coax array).

CONCLUSION

In conclusion, we have demonstrated a novel fabrication method for arrays of nanocoaxes using replicated arrays of silicon nanopillars in polymer, prepared by a stamp imprint technique. We modified the arrays to obtain arrays of open-ended, partially hollow nanocoaxes, with the coaxes' inner and outer electrodes serving as working and counter electrodes of a nanoscale electrochemical sensor. The width of the coax annulus controls the distance between electrodes in the sensor.

An observed increase in electrochemical signal with decrease of electrode distance (annulus width) is due to improvement in molecular diffusion, which depends inversely on electrode gap, robust radial diffusion ensured by the cylindrical geometry, and the high site density of nanoscale electrochemical sensors in the device. These result in a $\sim 100\times$ signal enhancement of the nanocoax over that of planar ES having millimeter separation between electrodes. Such a coaxial architecture can be employed to increase sensitivity of a range of electrochemical sensors, including label-free biosensors.

■ ASSOCIATED CONTENT

■ Supporting Information

Additional information as noted in text. This material is available free of charge via the Internet at <http://pubs.acs.org>.

■ AUTHOR INFORMATION

Corresponding Author

*E-mail: naughton@bc.edu. Fax: 617-552-8478.

Notes

The authors declare no competing financial interest.

■ ACKNOWLEDGMENTS

This work was supported by the National Institutes of Health (National Cancer Institute award No. CA137681 and National Institute of Allergy and Infectious Diseases award No. AI100216). Assistance from Dr. Gregory McMahon for FIB milling is acknowledged.

■ REFERENCES

- (1) Oja, S. M.; Wood, M.; Zhang, B. *Anal. Chem.* **2013**, *85*, 473–486.
- (2) Li, T.; Hu, W. *Nanoscale* **2011**, *3*, 166–176.
- (3) White, R. J.; White, H. S. *Langmuir* **2008**, *24*, 2850–2855.
- (4) Singh, K. V.; Whited, A. M.; Ragineni, Y.; Barrett, T. W.; King, J.; Solanki, R. *Anal. Bioanal. Chem.* **2010**, *397*, 1493–1502.
- (5) Bard, A. J.; Faulkner, L. R. *Electrochemical Methods*, 2nd ed.; Wiley: New York, 2001.
- (6) Mirkin, M. V.; Fan, F. R. F.; Bard, A. J. *J. Electrochem. Soc.* **1992**, *328*, 47–62.
- (7) Broers, A. N.; Lean, E. G.; Hatzakis, M. *Appl. Phys. Lett.* **1969**, *15*, 98–101.
- (8) Li, T.; Su, L.; Hu, W.; Dong, H.; Li, Y.; Mao, L. *Anal. Chem.* **2010**, *82*, 1521–1526.
- (9) Montelius, L.; Tegenfeldt, J. O.; Ling, T. G. I. *J. Vac. Sci. Technol.* **1995**, *13*, 1755–1760.
- (10) Zhang, H.; Chung, S.-W.; Mirkin, C. A. *Nano Lett.* **2003**, *3*, 43–45.
- (11) Fischbein, M. D.; Drndic, M. *Nano Lett.* **2007**, *7*, 1329–1337.
- (12) Gazzadi, G. C.; Angeli, E.; Facci, P.; Frabboni, S. *Appl. Phys. Lett.* **2006**, *89*, 173112–1–173112–3.
- (13) Nagase, T.; Kubota, T.; Mashiko, S. *Thin Solid Films* **2003**, *438*, 374–377.
- (14) Johnston, D. E.; Strachan, D. R.; Johnson, A. T. *Nano Lett.* **2007**, *7*, 2774–2777.
- (15) Park, H.; Lim, A. K. L.; Alivisatos, A. P.; Park, J.; McEuen, P. L. *Appl. Phys. Lett.* **1999**, *75*, 301–303.
- (16) Chen, F.; Qing, Q.; Ren, L.; Wu, Z.; Liu, Z. *Appl. Phys. Lett.* **2005**, *86*, 123105–1–123105–3.
- (17) Kim, J. H.; Moon, H.; Yoo, S.; Choi, Y. K. *Small* **2011**, *7*, 2210–2216.
- (18) Jung, M.; Song, W.; Sung Lee, J.; Kim, N.; Kim, J.; Park, J.; Lee, H.; Hirakawa, K. *Nanotechnology* **2008**, *19*, 495702.
- (19) Rizal, B.; Ye, F.; Dhakal, P.; Chiles, T. C.; Shepard, S.; McMahon, G.; Burns, M. J.; Naughton, M. J. In *Nano-Optics for Enhancing Light-Matter Interactions on a Molecular Scale*; Di Bartolo, B.,

Collins, J., Silvestri, L., Eds.; Springer: Dordrecht, Netherlands, 2013; pp 359–370.

(20) Rybczynski, J.; Kempa, K.; Herczynski, A.; Wang, Y.; Naughton, M. J.; Ren, Z. F.; Huang, Z. P.; Cai, D.; Giersig, M. *Appl. Phys. Lett.* **2007**, *90*, 021104–1–021104–3.

(21) Naughton, M. J.; et al. *Phys. Status Solidi-RRL* **2010**, *4*, 181–183.

(22) Paudel, T.; Rybczynski, J.; Gao, Y. T.; Lan, Y. C.; Peng, Y.; Kempa, K.; Naughton, M. J.; Ren, Z. F. *Phys. Status Solidi* **2011**, *A208*, 924–927.

(23) Zhao, H.; Rizal, B.; McMahon, G.; Wang, H.; Dhakal, P.; Kirkpatrick, T.; Ren, Z.; Chiles, T. C.; Naughton, M. J.; Cai, D. *ACS Nano* **2012**, *6*, 3171–3178.

(24) Choi, J.; Kenichi, S.; Kato, T. *Surf. Interface Anal.* **2010**, *42*, 1373–1376.

(25) Xia, Y.; Whitesides, G. M. *Annu. Rev. Mater. Sci.* **1998**, *28*, 153–184.

(26) Phosphate buffered saline 1X; Catalog No. BP2438-20; Fisher Scientific: 300 Industry Drive, Pittsburg, PA.

(27) Forster, R. J. *Chem. Soc. Rev.* **1994**, *23*, 289–297.

(28) Engstrom, R. C.; Weber, M.; Wunder, D. J.; Burgess, R.; Winquist, S. *Anal. Chem.* **1986**, *58*, 844–848.

(29) Robinson, R. S.; McCurdy, C. W.; McCreery, R. L. *Anal. Chem.* **1982**, *54*, 2356–2361.

(30) Sun, P.; Mirkin, M. V. *Anal. Chem.* **2006**, *78*, 6526–6534.

(31) Zevenbergen, M. A. G.; Wolfrum, B. L.; Goluch, E. D.; Singh, P. S.; Lemay, S. G. *J. Am. Chem. Soc.* **2009**, *131*, 11471–11477.

(32) Bi, S.; Liu, B.; Fan, F. R. F.; Bard, A. J. *J. Am. Chem. Soc.* **2005**, *127*, 3690–3691.

(33) Koehne, J.; Li, J.; Cassell, A. M.; Chen, H.; Ye, Q.; Ng, H. T.; Han, J.; Meyyappan, M. *J. Mater. Chem.* **2004**, *14*, 676–684.

(34) Parry, E. P.; Osteryoung, R. A. *Anal. Chem.* **1965**, *37*, 1634–1637.

(35) Wipf, D. O.; Bard, A. J. *J. Electrochem. Soc.* **1991**, *138*, 469–473.

(36) Fan, F. R. F.; Bard, A. J. *Science* **1995**, *267*, 871–874.

(37) Fan, F. R. F.; Bard, A. J. *Science* **1997**, *277*, 1791–1793.

(38) Lama, R. D.; Charlson, K.; Anantharam, A.; Hashemi, P. *Anal. Chem.* **2012**, *84*, 8096–8101.

SUPPORTING INFORMATION

A Nanocoax-Based Electrochemical Sensor

Binod Rizal¹, Michelle Archibald², Timothy Connolly², Stephen Shepard³, Michael J. Burns¹,
Thomas C. Chiles², and Michael J. Naughton^{1*}

¹Department of Physics, ²Department of Biology, ³Integrated Science Clean Room Facility
Boston College, Chestnut Hill, Massachusetts 02467, United States

*To whom correspondence should be addressed: naughton@bc.edu, Fax: 617-552-8478

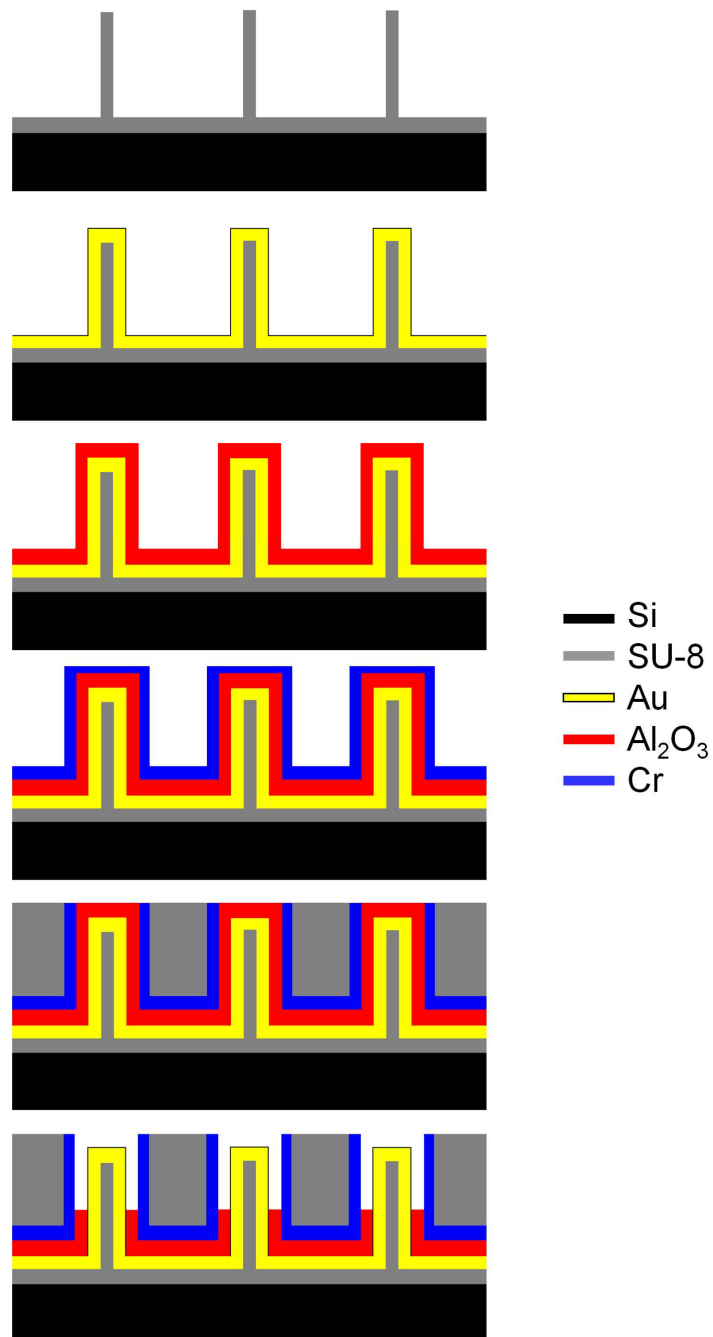


Figure S1. Schematic representations of fabrication process for nanocoax arrays. From top to bottom: polymer nanopillar array, inner metal coating, dielectric coating, outer metal coating, polymer coating and etching of dielectric.

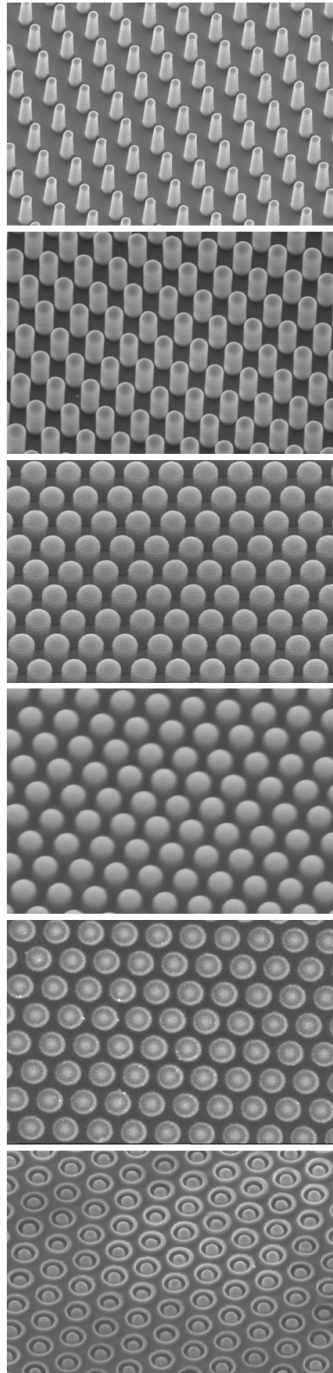


Figure S2. SEM images of the fabrication process for nanocoax structure of 1.3 μm pitch and 2 μm height. From top to bottom: inner metal coating, dielectric coating, outer metal coating, SU-8 coating, mechanical polishing and dielectric etching.

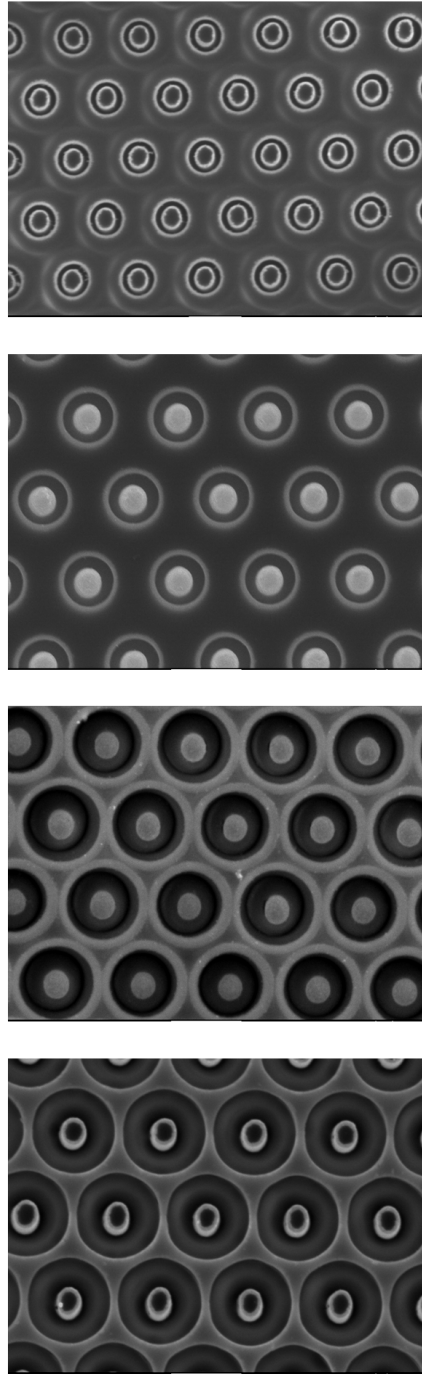


Figure S3. SEM images of nanocoax structure of 1.3 μm pitch and 500 nm annulus depth with different annulus thickness. From top to bottom: 100 nm, 200 nm, 300 nm and 400 nm.